TWO-PHASE FLOW BOILING IN MICROCHANNELS FOR COOLING OF MICROELECTRONICS

Thome J.R.* and Costa-Patry E.
*Author for correspondence
Heat and Mass Transfer Laboratory (LTCM)
Ecole Polytechnique Fédérale de Lausanne (EPFL)
1015 Lausanne
Switzerland,
E-mail: john.thome@epfl.ch

ABSTRACT

Recent progress in the study of two-phase flow boiling in single microchannels and multi-microchannels and the challenges posed by microelectronics cooling are reviewed. Experimental investigations have shown that uniform and transient heat fluxes and local hot-spots can be well handled by micro-evaporators. Furthermore, advances in the prediction of two-phase pressure drops and flow pattern transitions in microchannels are presented. The development of mechanistic models specific to the important flow regimes (elongated bubble flow and annular flow) opens the possibility for integrated flow pattern-based prediction methods. Presently two such methods are combined together to capture the transition between these two regimes and thus better predict the trends in the local flow boiling heat transfer process.

NOMENCLATURE

D	[m]	Diameter
G	[kg/m²s]	Mass flux
h	[kJ/kg]	Enthalpy
L	[m]	Length
P	[Pa]	Pressure
T	[°C]	Temperature

Special characters

	[W/m²K]	Heat transfer coefficient
	[kg/m³]	Density
μ	[Pas]	Kinematic viscosity

Subscripts

b	Base
chf	Critical heat flux
f	Fluid
j	Junction
l	Liquid
v	Vapor
w	Wall

Non-dimensional number

Bo	Boiling number $[q/Gh_{lv}]$
Co	Confinement number $[\sqrt{\sigma/D^2 g(\rho_l - \rho_v)}]$
Re	Reynolds number $[GD/\mu]$
We	Weber number $[G^2 D/\sigma\rho]$

INTRODUCTION

Air-cooled systems are commonly used for computers and power electronics. Koomey et al. [1] have calculated that the annual cost of running an air-cooled data center is currently as high as the annualized equipment costs. Air has a low specific heat so that large volumes have to be moved and chilled before entering the data centers. In turn, the power needed to operate the data centers rises rapidly and approaches close to 3% of the American electricity production (EPA report [2]).

Two-phase flow cooling is an optimal replacement for cooling of microelectronics. The refrigerant's latent heat of evaporation is much greater than the sensible heat of water, such that it requires a lower flow rate and less pumping power to remove the same amount of heat. In addition, the fluid temperature of two-phase flow is almost constant over the whole electronic surface whilst using a dielectric refrigerant removes the risk associated with water in an electrical circuit. Finally, two-phase cooling can be integrated in a heat pump cycle, which can efficiently increase the value of the waste heat by raising the system's output temperature for reuse.

Microelectronics is however challenging from a thermal point of view: it concentrates high heat fluxes on millimeter-sized surfaces. Current high-end CPU applications have a heat load of around 35W/cm², which is expected to rise in the next generation of chips to about 100-150 W/cm², while power electronics already generate heat fluxes above 120 W/cm². At the same time, in order to reduce risk of failure in micro-electronics nanometer-sized wires, the maximum chip temperature permissible is typically 85°C.

Putting these requirements in heat transfer terms, Fig 1 shows that for a footprint (base) heat flux of 140 W/cm^2, the footprint heat transfer coefficients have to be between 40'000 and 140'000 W/m^{2}K. If the ratio of actual surface in the microchannels to their footprint area is limited to 10, this corresponds to wall heat transfer coefficients of 4'000 to 10'000 W/m^{2}K.

To add to the complexity, CPUs have "hot-spots" in the core regions and lower heat fluxes in the cache and interconnect zones. The heat load also varies rapidly depending on the demand for computational power. Hamman et al. [3] found that the hot-spot to background heat flux ratios were around 10 to 1 and that the hot-spots covered 5 to 25% of the chip's area.

One last constraint is that the cooling system must be compact, which limits the channel size to a diameter of less than 3mm. At this size, bubbles generated by flow boiling start to be confined by the channel (and beneficially no stratified flow exists anymore) and microscale methods are needed to evaluate the flow behavior.

These microscale methods need first to be defined. For this aim, several studies have been performed. The first step was to evaluate the flow regimes found in two-phase microscale flow and to define where the transition between them happens. Then, it was important to study in which conditions critical heat flux occurs in microchannels in order to define safe operation limits.

On the modeling side, once the flow regimes are well defined, it is possible to develop pressure drop and heat transfer methods specifically for each flow regime. In the present case, the most important flow regimes are elongated bubble flow (called *coalescing bubble* here since it includes the bubble-to-slug flow transition where short bubbles still exist) and annular flow.
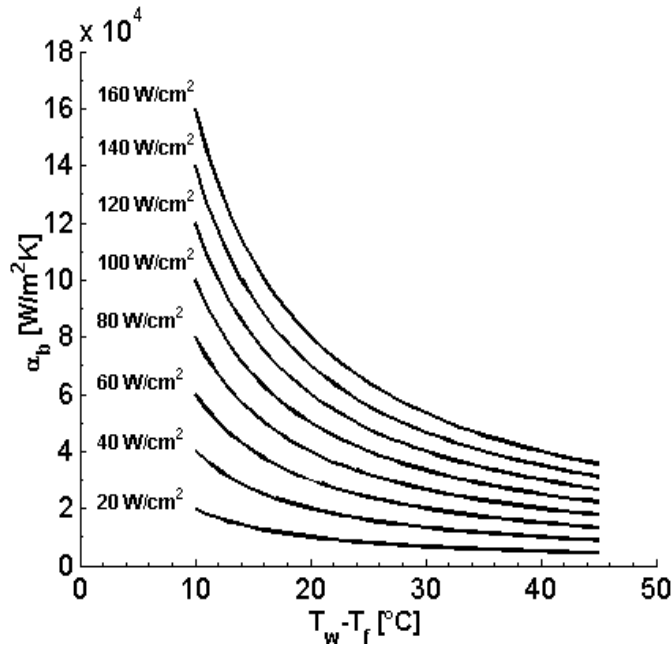
For the hydraulic and thermal design of a micro-evaporator, an extensive experimental database has been collected on pressure drop and heat transfer coefficients, both under uniform and non-uniform heat flux conditions. Transient heat flux conditions were also tested to assess the response of the evaporator to a sudden change in heat flux.

The objectives of the present paper are to present the progress made in the study of two-phase flow boiling in microchannels, describe the most recent pressure drop and heat transfer prediction methods developed for these conditions and show how two-phase flow boiling can be applied to microelectronics cooling. It will be based nearly exclusively on work performed and methods developed in the LTCM laboratory covering extensive test conditions, with the present paper pulling much of this work into one unified paper.

FLOW REGIMES AND FLOW PATTERNS MAPS

The study of two-phase flow patterns describe how the liquid and vapor phase are distributed in the channel. Each specific flow configuration will affect its thermal and hydraulic characteristics. In order to determine microchannel flow patterns, long circular glass tubes of diameter larger than 500μm were used. Revellin et al. [4] found three stable flow regimes: bubbly flow, slug flow and annular flow. These were separated by transition zone of bubbly-slug flow and slug-annular flow. All are depicted in Fig 2.

In Fig 3, Ong and Thome [5]'s flow pattern map shows where each flow regime is present. The bubbly and slug flow (the latter includes the bubbly-slug transition) regimes were renamed respectively isolated and coalescing bubble flow.

Two transition lines were defined. The isolated to coalescing bubbles transition (IB–CB) was found to happen when the vapor quality was:

$$x_{IB-CB} = 0.36 Co^{0.3} \left(\frac{\mu_v}{\mu_l}\right)^{0.65} \left(\frac{\rho_v}{\rho_l}\right)^{0.9} \frac{Re_v^{0.75} Bo^{0.25}}{We_l^{0.91}} \qquad (1)$$

The transition between coalescing bubbles and annular flow happened at:

$$x_{CB-A} = 0.047 Co^{0.05} \left(\frac{\mu_v}{\mu_l}\right)^{0.7} \left(\frac{\rho_v}{\rho_l}\right)^{0.6} \frac{Re_v^{0.8}}{We_l^{0.91}} \qquad (2)$$

Four non-dimensional numbers are used in these equations:

1. *Co*, Confinement number: ratio of the surface tension and buoyancy forces;
2. *Re$_v$*, Reynolds number: ratio of the inertia to the viscous forces;
3. *We$_l$*, Weber number: ratio of inertia to the surface tension forces;
4. *Bo*, Boiling number: ratio of the heat flux to the heat of vaporization.

Figure 1 Required base heat transfer to maintain the chip temperature below 85°C for different heat fluxes

The Confinement number is also a good indicator of the two-phase macro- to microscale transition, which can be defined as the point where the channel dimension modifies the flow behavior. In a macroscale flow, bubbles slide along the top wall due to buoyancy. As the channel diameter decreases, the importance of the surface tension increases and some point the bubble "fills" the cross-section of the channel surrounding by a thin liquid film.

Ong and Thome [5] found that the liquid film surrounding a bubble was symmetric for Co > 1. At this point, gravity is a weak force compared to surface tension. There is then a transition as the channel diameter is increased, during which buoyancy effect becomes more important, until about Co < 0.3, where gravity clearly dominates surface tension.
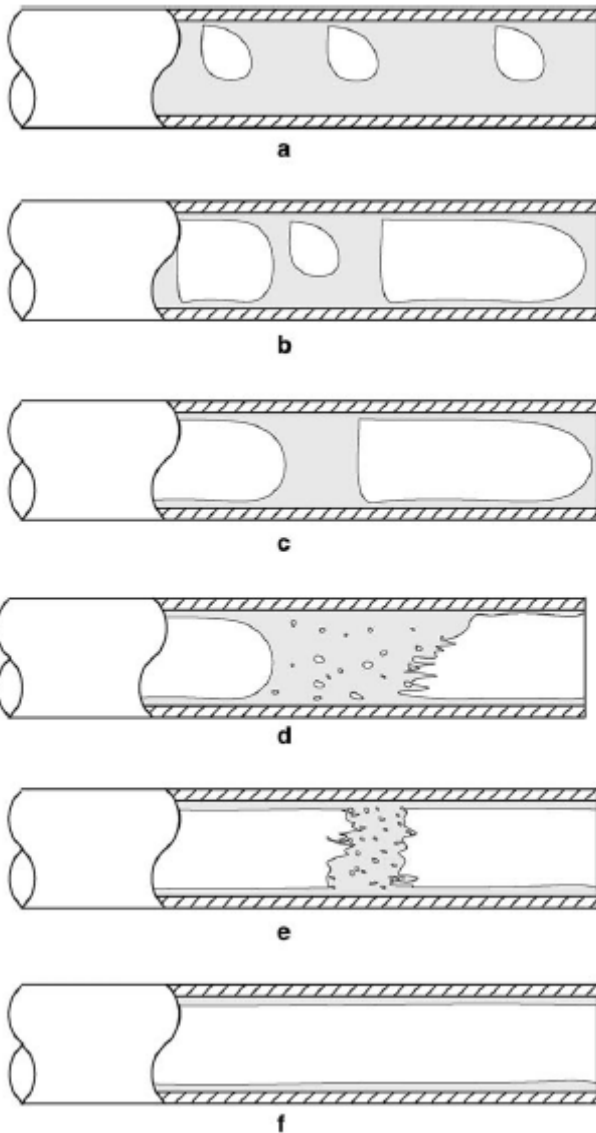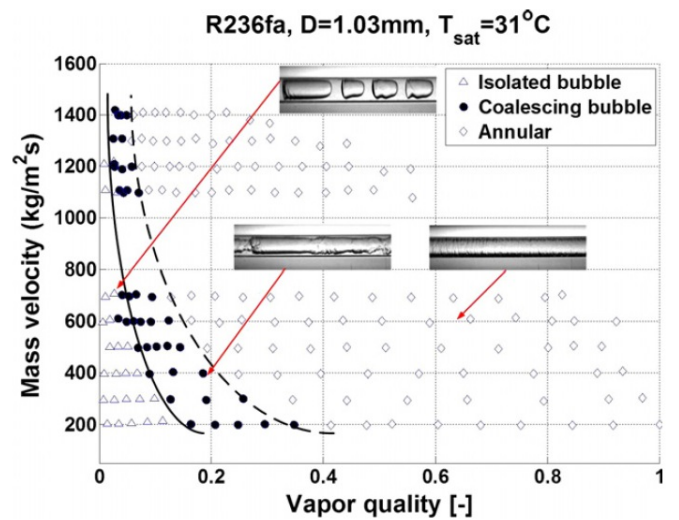

Figure 3 Flow pattern map. From Ong and Thome [5].

CRITICAL HEAT FLUX

One last transition is needed in the flow pattern map shown in Fig 3, that is the dry-out or critical vapor quality given by the critical heat flux. Since staying below the critical heat flux (CHF) is an important thermal safety criterion, defining it received a lot of attention. Ong and Thome [6] and Wojtan et al. [7] made together a total of 215 critical heat flux measurements with R-134a, R-236fa and R-245fa in single tube microchannels. Park and Thome [8] made 323 measurements in copper multi-microchannels. Using the same multi-microchannels in split flow configuration, Mauro et al. [9] made 78 measurements. The empirical prediction method of Wojtan et al. [7] was found to be in good agreement with these experiments:

$$q_{CHF} = 0.437 \left(\frac{\rho_v}{\rho_l}\right)^{0.073} We_l^{-0.24} \left(\frac{L}{D}\right)^{-0.72} Gh_{lv} \quad (3)$$

For the same conditions as given in Fig 3, the critical heat flux value would be 8.5 W/cm^2 for a mass flux of 600 kg/m^{2}s while 10.8 W/cm^2 for 1000 kg/m^{2}s. Note that high aspect rectangular channel gives a much larger footprint CHF, since to obtain the footprint CHF, the wall-based value need to be multiplied by the area ratio corrected for fin efficiency.

The heated length is very important in the Wojtan et al. [7]'s correlation, as it is used in the Weber number definition and in L/D. Thus shorter evaporators have much higher critical heat flux and at the microelectronics scale (less than 20mm), wall critical heat flux levels are closer to 40 W/cm^2 ($q_{chf-base}$= 400 W/cm^2).

PREDICTION METHODS FOR SPECIFIC FLOW REGIMES

Looking at Fig 2, the distribution of the vapor and liquid phases are very different between flow patterns. The succession of liquid and vapor slugs will generate a pressure drop and lead to heat transfer different to what is found in the continuous liquid film in annular flow. This is why mechanistic modeling of two-phase flow in microchannel is made for specific flow regimes.

Figure 2 Schematic of flow pattern. From Revellin et al. [4]

Pressure drop prediction methods

For two-phase pressure drop in microchannels, a mechanistic model was developed for circular channel annular flow by Cioncolini et al. [10] and was tested for channel diameters as small 0.5 mm. They proposed a new one-dimensional turbulence model for macro and microscale two-phase annular flow. As shown in Fig 4, it separated the channel cross-section into the liquid film, the vapor core and the entrained liquid. The model can be used to predict the frictional pressure gradients, the liquid velocity profile in the annular film, the film thickness, the fraction of liquid entrained in the vapor core and the void fraction. As it is not applicable to other flow regimes, another prediction method must be used for intermittent flow regimes, for example the separate flow model of Lockhart and Martinelli [17]. Ong and Thome [5]'s CB–A transition can be used to change from one to the other.
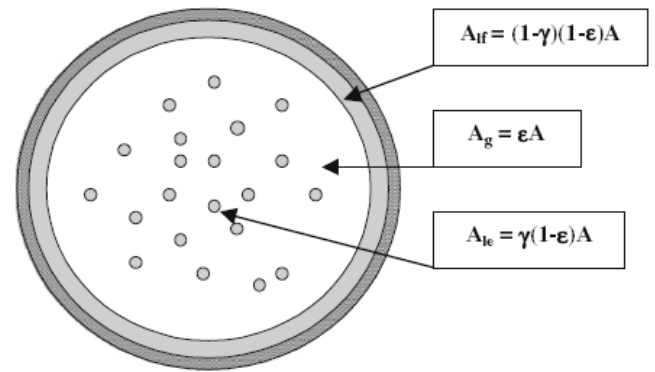
Heat transfer coefficient prediction methods

Two mechanistic prediction methods, each valid in microchannel, have been developed for two-phase heat transfer coefficients: the three-zone model for intermittent flow regimes (i.e. isolated bubble and coalescing bubble flow regimes) and one for annular flow.

The three-zone model was developed by Thome et al. [12] as a semi-mechanistic model, describing the evaporation of elongated bubbles in microchannels. Fig 5 shows the schematic of their model. Bubbles form at a given frequency (f) and are separated by liquid slugs. The bubbles grow and form a film with an initial thickness δ_0. The rate of vapor formation is tracked and if, as the bubble grows, the liquid film surrounding the bubble reaches a minimum value ($_{min}$), the evaporating film is assumed to dry out and form a vapor slug (dry zone) behind the elongated bubble.

The heat transfer coefficients in the liquid and vapor slug are evaluated using a laminar and turbulent developing flow correlation. Heat transfer in the elongated bubble happens through thin film evaporation, which is modeled by one-dimensional conduction through the film. Finally, the cyclical variation of the heat transfer due to the different zones is used to obtain a time-averaged heat transfer coefficient. The method requires f, $_0$ and $_{min}$ to be modeled. Agostini et al. [13], Ong and Thome [6] and Costa-Patry et al [18] showed that setting the minimum film thickness to the channel wall roughness improved the accuracy of the method.

Although heat transfer in annular flow appears at first look to be similar in macro- and microscale, since the liquid film thickness at both scales are much smaller than the channel diameter, they nevertheless differ in some aspects. The liquid film is thinner and can be laminar, which affects the liquid-vapor interface interactions. Moreover, since the surface tension is more important in a microchannel, a non-circular channel will proportionally concentrate more liquid in its corners, thin the film and increase heat transfer, as it was shown by Nebuloni [14] through numerical simulation of condensing laminar annular flow.
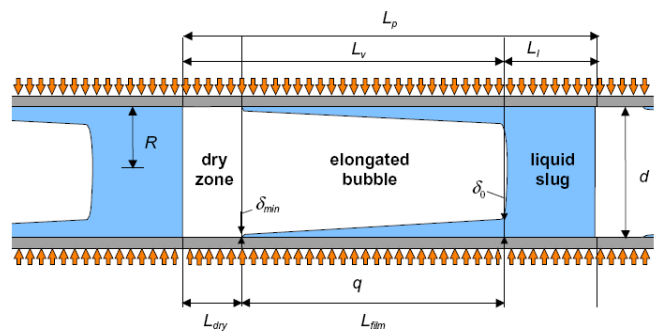

Figure 4 Annular flow cross-section. From Cioncolini et al. [10]

Figure 5 Schematic of the three-zone model of Thome et al. [12]

The annular flow heat transfer prediction method of Cioncolini and Thome [15] covers macro and microscales. It is derived from a mechanistic analysis of the annular flow and used experimental results from 1.03 to 14.4 mm circular test sections to optimize the method's accuracy. It provides information about the film velocity and temperature profiles, the average film thickness, the void fraction and the heat transfer coefficient.

With these two models, a transition criterion from intermittent to annular flow is needed to create a flow pattern-based method. In Fig 6 are plotted the prediction of the three-zone and the annular flow model for a flow of R-236fa in a circular pipe of 500 μm diameter with Ong and Thome [5]'s CB–A transition. The heat transfer values predicted by the three-zone model increase with the heat flux, whereas the annular flow model is insensitive to heat flux. The three-zone line then crosses the annular flow lines at higher vapor qualities as the heat flux is increased. Using the CB–A transition criterion would lead to a sudden change in evolution of the heat transfer, since it predicts a transition at x = 0.18 for all heat fluxes.
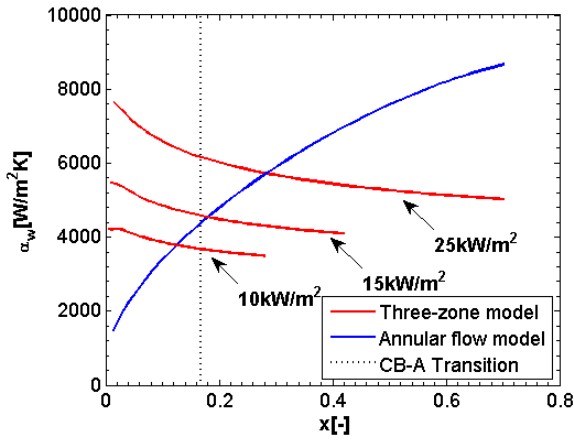
Figure 6 Heat transfer coefficient prediction of the three-zone and annular flow models.

TWO-PHASE EXPERIMENTS IN MICRO-EVAPORATORS

To cool microelectronic components, evaporators are typically composed of several parallel microchannels all connected to common inlet and outlet plenums. The fluid enters the inlet plenum in liquid phase, starts boiling in the channels and it collected at the channel end in the outlet plenum. A heater is placed at the base of the evaporator and local temperature sensors are typically placed on the heater.

It is important to ensure a uniform flow distribution between all channels, since measuring the flow condition in each channel is not feasible. Park et al. [16] have shown that placing small orifice in front of each channel stabilizes the flow distribution. This orifice can also be a geometrical reduction or a change of flow direction, as done by Agostini et al. [13], the objective being to prevent backflows of vapor into the inlet plenum. If the subcooling in the inlet plenum is low, the inlet restriction also serves to start the boiling process by flashing.

Using this knowledge, Costa-Patry et al. [17] developed a test chip to mimic the thermal behavior of computer chips. It was composed of 35 heaters, each having its own thermal sensor. This setup allowed non-uniform and transient heat fluxes to be applied, since each heater could be independently controlled. In total, 70 heat flux and temperature measurements were acquired simultaneously. On top of the test chip, a silicon micro-evaporator was placed, composed of 135 channels, each 85μm wide, 560 μm high and separated by 46 μm fins. A good thermal contact between both surfaces was made by using a high thermal conductivity liquid metal as the interface material.

Pressure drop measurements

Micro-evaporators usually have a hydraulic diameter smaller than 500 μm and direct pressure measurements in such channels are difficult. These are then usually made in the larger inlet and outlet plenums and not directly in the channel. The total pressure, measured between the plenums, can be divided into three components:

$$dP_{total} = dP_{restr-in} + dP_{ch} + dP_{restr-out}$$

Since the flow entering the inlet restriction is single-phase and the effect of flashing is small, $dP_{restr-in}$ can be calculated from single-phase pressure drop correlations. On the other end, $dP_{restr-out}$ is two-phase and difficult to predict. Costa-Patry et al. [17] developed a method to measure this quantity. Their evaporator was able to be heated by sections and the first part was heated to generate a two-phase flow. The heat-spreading within the evaporator was limited (based on analysis) and the last part of the evaporator was adiabatic. The temperature sensors in this zone then measured the local fluid saturation temperature (and thus local saturation pressure), which made it possible to evaluate the outlet restriction pressure drop. The same measurement technique was also used to show that pressure drops from the inlet plenum to seven measurement points placed at the same downstream position but at different lateral position varied by less than 5%, indirectly proving that the flow was uniformly distributed across all channels.

Fig 7 shows that the inlet and outlet restrictions contribute in non-negligible amount of the total pressure drop. For low mass flux the outlet restriction can lead to pressure recovery.
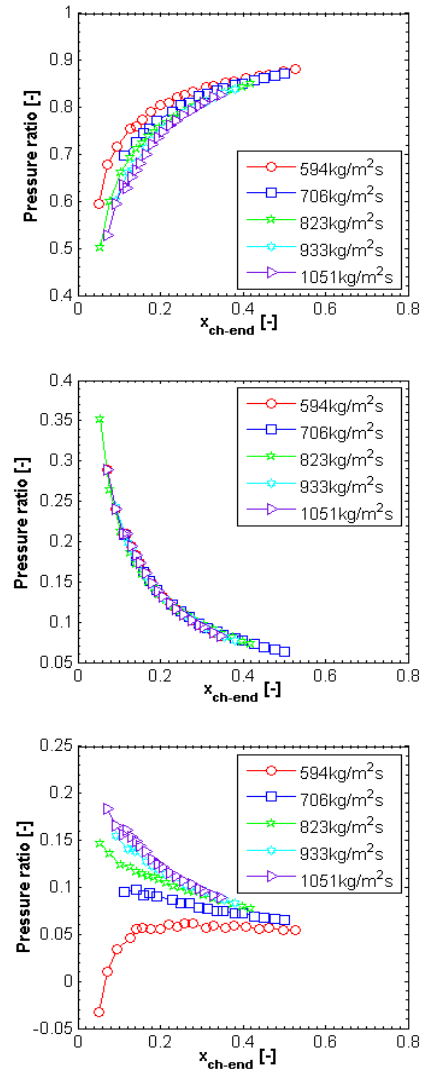

Figure 7 Pressure drop ratio for R-236fa. Top: Channel. Middle: Inlet restriction. Bottom: Outlet restriction. From Costa-Patry et al. [17]
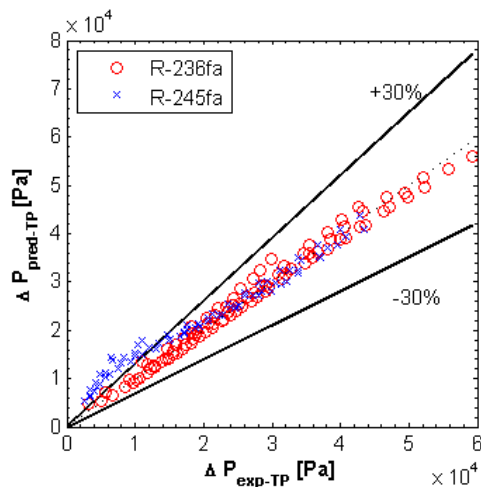
Figure 8 Accuracy of Cioncolini et al. [10] pressure drop method versus results from Costa-Patry et al. [Pa]

Figure 9 Heat transfer coefficient for HFC-152a. From Hamdar et al. [22]

To determine wall heat transfer coefficients in a microchannel, the external wall temperatures and the inlet and the outlet pressure measurements must be converted into internal wall and local fluid temperatures. This data processing involves a few assumptions. The local fluid temperatures are typically calculated by imposition a linear pressure drop from the onset of boiling point to the end of the channel. Costa-Patry et al. [18] has shown that depending on the outlet quality and the refrigerant, this assumption can lead at most to a 15% difference in local heat transfer coefficient, when compared to the results obtained using the Cioncolini et al. [10] annular flow pressure drop prediction method.

The internal wall temperature is typically determined using one-dimensional heat conduction. For the uniform heat flux condition, Costa-Patry et al. [19] have shown that this assumption was as precise as using a multi-dimensional heat conduction scheme. Finally, to determine the wall heat flux in multi-microchannels, fin theory is used (Kreith and Bohn [20]).

Although the data reduction is similar in most studies, the experimental heat transfer results can be very different. Thome and Consolini [21] placed experimental trends reported for microscale heat transfer coefficients in several groups. In some studies, the heat transfer coefficient was found to be unaffected by the vapor quality or the mass flux, but strongly dependent on the heat flux. An example of this trend is given in Fig 9 by Hamdar et al. [22] with HFC-152a in a 1 mm tube.

In a second group of studies, heat transfer coefficients were found to be a function of the vapor quality and the heat flux. The Lin et al. [23] graph for R-141b in a 1 mm tube, reproduced in Fig 10, show the variation of heat transfer coefficient with respect to heat flux and vapor quality. As the heat flux increases, the mean heat transfer increases. First the local heat transfer tends to be higher towards the end of the channel, at high vapor qualities, but at higher heat flux, the shape of the curve changes. It flattens and later has a decreasing trend with vapor quality.
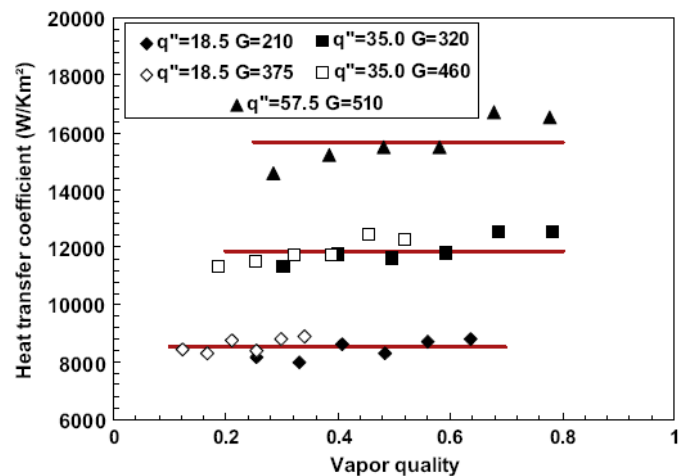
The two first trends are clearly seen in the results of Costa-Patry et al. [18] obtained in a multi-microchannels. In Fig 11, the evolution of the heat transfer coefficients for R-236fa at 1051 kg/m²s are reproduced. For the same conditions, the heat transfer coefficients predicted by the combination of the three-zone and the annular flow heat transfer models are plotted in Fig 12. The experimental vapor qualities were used for the calculations, which explains the low resolution of the graph.

The annular flow model is here implemented by spreading the liquid film calculated for the circular channel geometry of the Cioncolini and Thome [15] model to the wetted perimeter of the rectangular channel, specific details are given in Costa-Patry et al. [19].

The predictions overestimate the heat transfer coefficients by about 30%. However, the transitions occur almost at the same vapor qualities and the shape of the curve is well predicted. This result supports the idea of developing flow-pattern based prediction methods. It would be preferable to base the transition on direct observation of the flow, such as done by Ong and Thome [5], but their criterion would need to be improved by including a heat flux dependency on their CB–A transition.
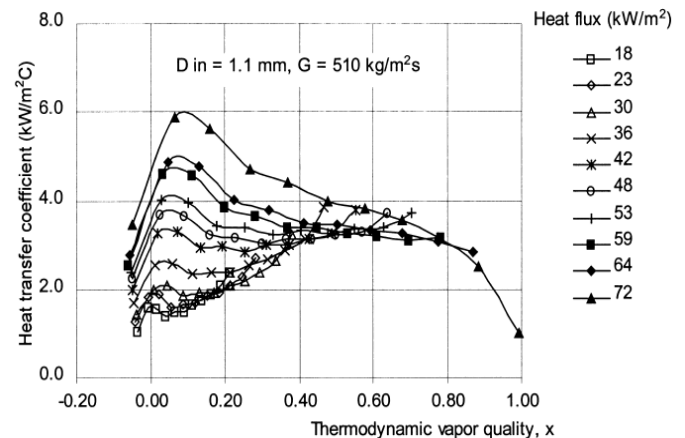

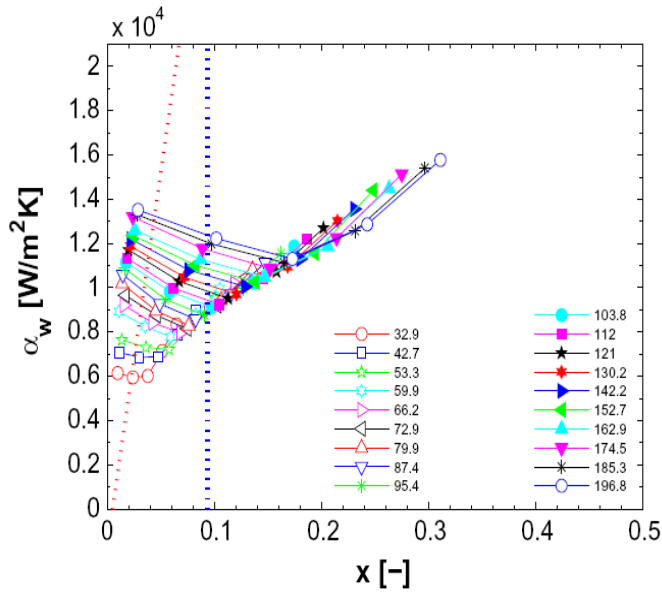**Figure 10 Heat transfer coefficient for R-141b. From Lin et al. [23]**

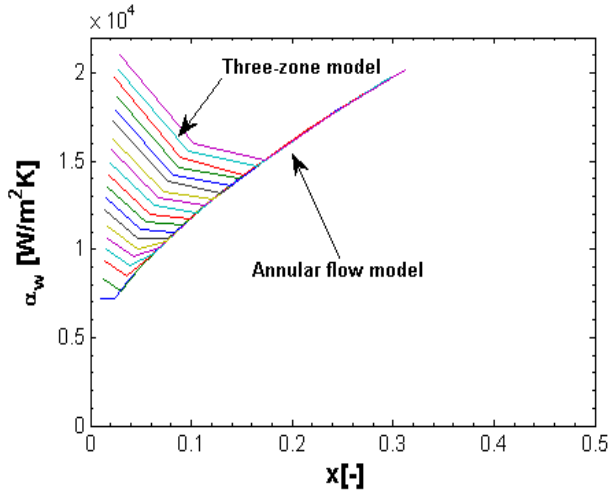**Figure 11 Heat transfer coefficient for R-236fa at 1051 kg/m²s. From Costa-Patry et al. [18]**

Figure 12 Prediction of combined three-zone and annular flow models for R-236fa at 1051 kg/m²s.

Experimental study of hot-spots in micro-evaporators

Microelectronics generates a non-uniform heat flux, where the peak heat flux can be ten times higher than the background one. Two-phase flow cooling is often seen as a good candidate for hot-spot cooling, because its heat transfer is a strong function of the heat flux, but this has not been studied in detail.

The test vehicle developed by Costa-Patry et al. [17] was able to mimic these characteristics. An example of the power and temperature maps found at the base of the test section is given in Fig. 13. In the graph, the highest heat flux stands for the hot-spot heat flux and the other is the background heat flux. Note that some temperature sensors were not functional, whereas all heaters were working.
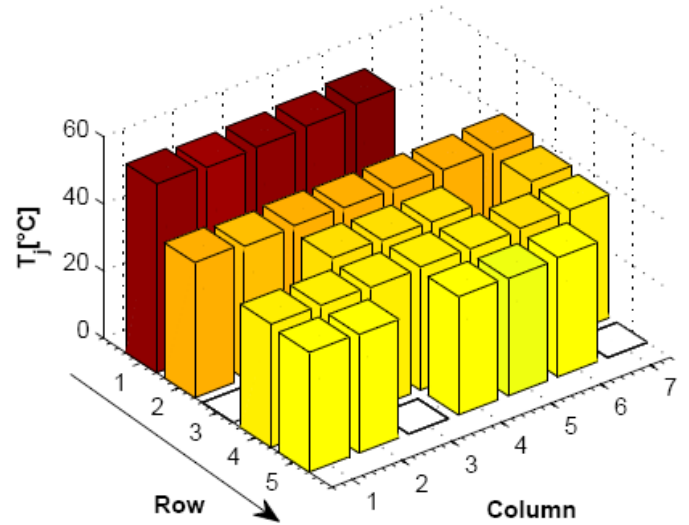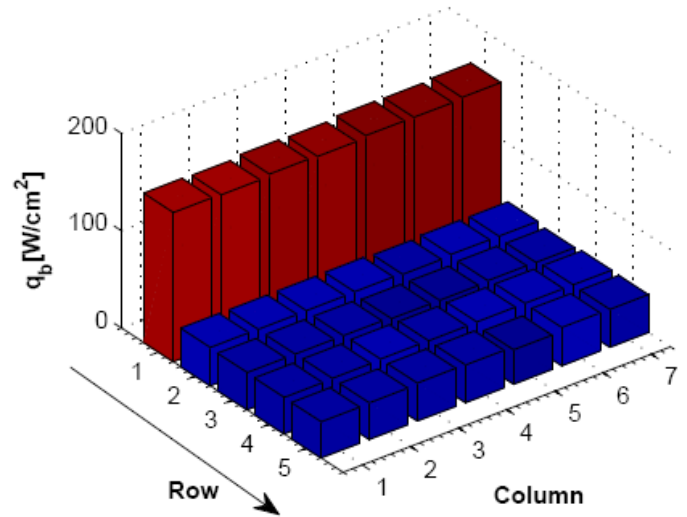

Figure 13 Power and temperature map for hot-spot at inlet row. From Costa-Patry et al. [19]

Fig 14 shows the heat transfer coefficient changes when the same heat flux level is distributed along different downstream positions. In Fig 15 heat transfer coefficient results for uniform and non-uniform heat flux are compared. When the hot-spot is positioned at the outlet (R5H), local heat transfer coefficients can be predicted from the corresponding value at the same vapour quality and heat flux. However, when the hot-spot is placed at the inlet (R1H), uniform and non-uniform heat transfer results do not matched because the vapor quality does not describe completely the fluid state and its behavior.

As it was previously discussed, two-phase heat transfer in microchannels depends on the local flow pattern. The effect of the hot-spot on the flow pattern is difficult to assess, but if the hot-spot is placed at the inlet, it is probable that it increases the bubble frequency, thus increasing further downstream the local heat transfer coefficients over the zone of lower heat flux as per the three-zone model predictions.

It is then preferable to position a hot-spot close to the inlet of the test section, since the average heat transfer coefficient of the evaporator will be higher. One disadvantage would be an increase in the total pressure drop, which can be problematic for applications where the available pressure is limited. Furthermore, the annular flow heat transfer coefficient is essentially insensitive to heat flux while the three-zone model gives a "nucleate pool boiling" type of rise in its local value, hence better local cooling is provided under hot-spots at low vapor qualities.
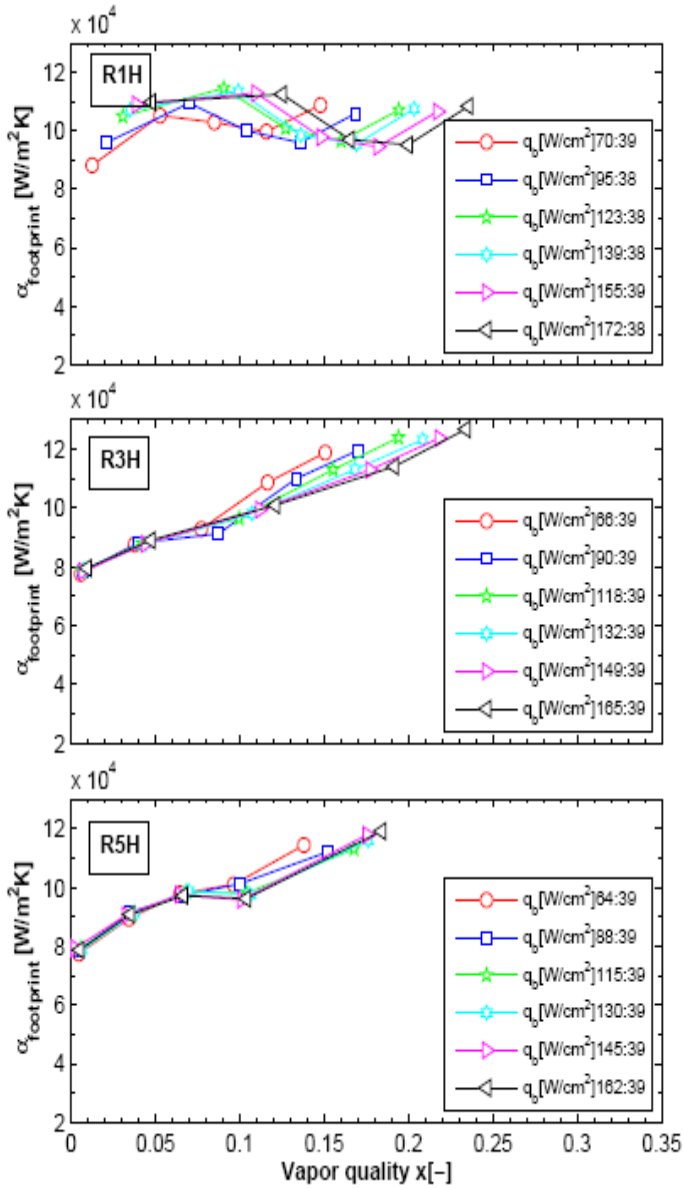

Figure 14 Heat transfer coefficients for varying row hot-spots and constant background heat flux, G=500 kg/m²s. From Costa-Patry et al. [19]
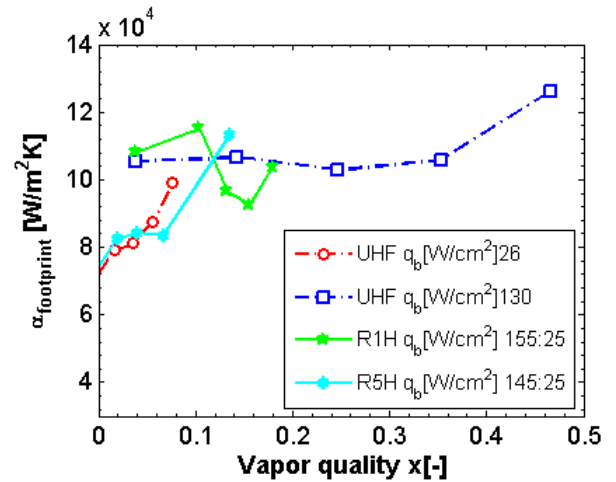

Figure 15 Heat transfer coefficient comparison between uniform and non-uniform heat flux. From Costa-Patry et al. [19]

Transient heat fluxes

In CPUs, the heat generation follows the computational duty. Since the CPU clock speed is on the order of mega- and gigahertz, instantaneous local heat flux variation is very fast. However, from a cooling requirement point of view, the time scale is longer. Hamman et al. [3] showed than when a CPU starts, the chip temperatures first increased in a step function and then remained mostly stable.

Using a copper micro-evaporator and the same test setup as Costa-Patry et al. [17], the base heat flux was varied in a series of square waves. The resulting heat flux and temperature traces are shown in Fig 16. The base heat flux varies from 75 W/cm² and 130 W/cm² in intervals of one second. The temperature trace follows the heat flux closely. It varies between 42°C and 49°C and the mean value does not increase with time. This shows that the cooling response of the micro-evaporator is fast and that a sudden increase or decrease in heat flux does not destabilize the system.
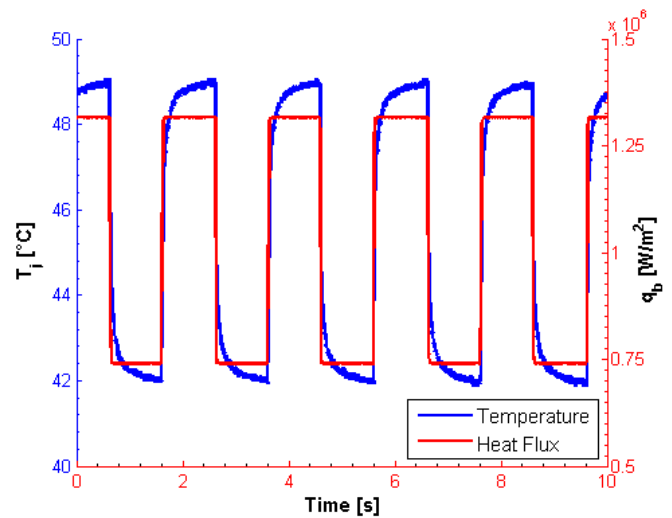

Figure 16 Heat flux and temperature trace under transient heat flux.

CONCLUSION

Much progress has been made on two-phase flow boiling in microchannels to allow detailed thermal and hydraulic analysis of micro-evaporators. The development of pressure drop and heat transfer prediction methods for specific flow regimes points toward integrated prediction methods covering all flow patterns.

Based on experimental results in heat transfer coefficients, existing transition criteria need to be modified, since they do not include the effect of heat flux. Micro-evaporators can efficiently handle the challenges posed by microelectronics cooling: cooling of uniform heat fluxes, hot-spots and transient heat fluxes was done without any difficulty and the base critical heat fluxes can be over 300 W/cm^2.

REFERENCES

[1] Koomey, J., Belady, C., Patterson, M., Santos, A. and K.D., Lange. Assessing trends over time in performance, costs, and energy use for servers. *Lawrence Berkeley National Laboratory and Stanford University*. 2009

[2] United States of America Environmental Protection Agency, Report to Congress on Server and Data Center Energy Efficiency. 2007

[3] Hamann, H., Weger, A., Lacey, J., Hu, Z., Bose, P., Cohen, E. and Wakil, J. Hotspot-Limited Microprocessors: Direct Temperature and Power Distribution Measurements *IEEE J. Solid-State Circuit*, 2007*, 42(1)*, 56-65

[4] Revellin, R. and Thome, J.R. A new type of diabatic flow pattern map for boiling heat transfer in microchannels. *J. Micromech. Microeng.*, 2007*, 17*, 788-796

[5] Ong, C. and Thome, J.R. Macro-to-microchannel transition in two-phase flow: Part 1 - Two-phase flow patterns and film thickness measurements. *Exp. Therm. Fluid Science*, 2011*, 35*, 37-47

[6] Ong, C. and Thome, J.R. Macro-to-microchannel transition in two-phase flow: Part 2 - Flow boiling heat transfer and critical heat flux *Exp. Therm. Fluid Science*, 2011

[7] Wojtan, L., Revellin, R., Thome, J.R. Investigation of saturated critical heat flux in a single, uniformly heated microchannel *Exp. Therm. Fluid Science*, 2006*, 30*, 765-774

[8] Park, J. and Thome, J.R. Critical heat flux in multi-microchannel copper elements with low pressure refrigerants *Int. J. Heat Mass Transfer*, 2010*, 53*, 110-122

[9] Mauro, A., Thome, J.R., Toto, D. and Vanoli, G. Saturated critical heat flux in a multi-microchannel heat sink fed by a split flow system *Exp. Therm. Fluid Science*, 2010*, 34*, 81-92

[10] Cioncolini, A., Thome, J.R. and Lombardi, C. Unified macro-to-microscale method to predict two-phase frictional pressure drops of annular flows *Int. J. Multiphase Flow*, 2009*, 35*, 1138-1148

[11] Lockhart, R. and Martinelli, R. Proposed correlation of data for isothermal two-phase, two-component flow in pipes *Chem. Eng. Prog.*, 1949*, 45*, 39-48

[12] Thome, J.R., Dupont, V. and Jacobi, A. Heat transfer model for evaporation in microchannels. Part I: presentation of the model *Int. J. Heat Mass Transfer*, 2004*, 47*, 3387-3401

[13] Agostini, B., Revellin, R., Thome, J.R., Fabbri, M., Michel, B., Calmi, D. and Kloter, U. High heat flux flow boiling in silicon multi-microchannels – Part I: Heat transfer characteristics of refrigerant R236fa *Int. J. Heat Mass Transfer*, 2008*, 51*, 5400-5414

[14] Nebuloni, S. and Thome, J.R. Numerical modeling of laminar annular film condensation for different channel shapes *Int. J. Heat Mass Transfer*, 2010*, 53*, 2615-2627

[15] Cioncolini, A. & Thome, J.R. Algebraic turbulence modeling in adiabatic and evaporating annular two-phase flow *Under review Int. J. Heat Fluid Flow*, 2011

[16] Park, J., Thome, J.R. and Michel, B. Effect of Inlet Orifice on Saturated CHF and Flow Visualization in Multi-microchannel Heat sinks *25th IEEE SEMI-THERM Symposium*, 2009

[17] Costa-Patry, E., Olivier, J., Nichita, B., Michel, B. and Thome, J.R. Two-phase flow of refrigerants in 85um-wide multi-microchannels: Part I – Pressure drop *Int. J. Heat Fluid Flow*, 2011*, 32(2)*, 451-463

[18] Costa-Patry, E.; Olivier, J.; Michel, B. and Thome, J.R. Two-phase flow of refrigerants in 85um-wide multi-microchannels: Part II: Heat transfer with 35 local heaters *Int. J. Heat Fluid Flow*, 2011*, 32(2)*, 464-476

[19] Costa-Patry, E., Nebuloni, S., Olivier, J. and Thome, J.R. On-chip two-phase cooling with refrigerant 85 um-wide multi-microchannel evaporator under hot-spot conditions *Submitted to IEEE Trans. Components and Packaging Tech.*, 2011

[20] Kreith, F. and Bohn, M. Principles of Heat Transfer *Brooks/Cole*, 2001

[21] Thome, J.R. and Consolini, L. Mechanisms of Boiling in Micro-Channels: Critical Assessment *Heat Transfer Eng.*, 2009*, 31*, 288-297

[22] Hamdar, M.; Zoughaib, A. and Clodic, D. Flow boiling heat transfer and pressure drop of pure HFC-152a in a horizontal mini-channel *Int. J. Refrigeration*, 2010*, doi:10.1016/j.ijrefrig.2009.12.006*, 1-12

[23] Lin, S.; Kew, P. and Cornwell, K. Two-phase heat transfer to a refrigerant in a 1 mm diameter tube *Int. J. Refrigeration*, 2001*, 24*, 51-56